Journal of Solid State Chemistry **147,** 631–636 (1999)
Article ID jssc.1999.8427, available online at http://www.idealibrary.com on IDEAL®

Structure and Oxide Ion Conductivity Mechanism in $Bi_2Al_4O_9$ by Combined X-Ray and High-Resolution Neutron Powder Diffraction and ^{27}Al Solid State NMR

I. Abrahams,*,[1] A. J. Bush,* G. E. Hawkes,* and T. Nunes†

*Structural Chemistry Group, Department of Chemistry, Queen Mary and Westfield College, University of London, Mile End Road, London E1 4NS, United Kingdom; and †Departamento de Engenharia de Materiais, Instituto Superior Tecnico, Av. Rovisco Pais, 1096 Lisboa Codex, Portugal

Received March 29, 1999; in revised form June 4, 1999; accepted June 8, 1999

The structure of $Bi_2Al_4O_9$ has been refined using a combination of X-ray and high-resolution neutron powder diffraction. Iterative simulation of the ^{27}Al MAS solid state NMR data confirms the presence of two Al sites, one octahedral and one tetrahedral, in an approximate 1:1 ratio. The structure of $Bi_2Al_4O_9$ has been refined anisotropically in the orthorhombic space group *Pbam*, with $a = 7.7134(1)$, $b = 8.1139(2)$, $c = 5.6914(1)$ Å, and $Z = 2$. The refinement terminated with $R_{wp} = 17.09\%$ (X ray), 11.44% (neutron); $R_{ex} = 4.52\%$ (X ray), 3.22% (neutron). The structure consists of edge-sharing columns of AlO_6 octahedra running parallel to the *c*-axis. These columns are linked by pairs of apex sharing AlO_4 tetrahedra, with Bi atoms located between the columns. The Bi $6s^2$ lone pairs point toward vacant sites in the structure. A one-dimensional conductivity mechanism along the *c*-axis vector is proposed involving these sites.

INTRODUCTION

There has recently been considerable interest in bismuth oxide based compounds for applications in solid oxide fuel cells, oxygen sensors, and gas separation membranes (1). There have been several reports concerning the bismuth aluminate system $Bi_2Al_4O_9$ (2–4). The Bi–Al–O phase diagram (2) indicates that two compounds are formed in the system: $BiAlO_3$ and $Bi_2Al_4O_9$. However, Bloom *et al.* question the stability of the former (4). The crystal structure of $Bi_2Al_4O_9$ was originally solved by single-crystal X-ray diffraction (3). In considering this material as an oxide ion conductor an accurate picture of the anion sublattice is required. In $Bi_2Al_4O_9$, X-ray scattering is dominated by the heavy atom bismuth. By using a combination of X-ray and neutron diffraction, both heavy atom (Bi) and light atom (Al, O) positional and thermal parameters can be determined accurately. In addition, the use of ^{27}Al solid state NMR data gives detailed information on the Al coordination which can be compared with other aluminate systems.

The electrical behavior of $Bi_2Al_4O_9$ has been investigated by Bloom *et al.*, who found conductivity values on the order of 10^{-2} S cm^{-1} at 800°C (4).

EXPERIMENTAL

Preparation

Polycrystalline $Bi_2Al_4O_9$ was prepared from Bi_2O_3 (Avocado, 99%) and α-Al_2O_3 (Aldrich, 99%) by conventional solid state techniques. Starting materials were ground as a slurry in ethanol using an agate mortar and pestle. The dried mixture was placed in a platinum crucible and heated in air at 700°C for 3 h and then for 12 h at 865°C. The sample was then rapidly quenched in air onto a stainless steel plate. Phase purity was determined by X-ray powder diffraction.

Crystallography

X-ray diffraction data were collected at room temperature on a Siemens D5000 X-ray powder diffractometer with secondary beam graphite monochromated Cu$K\alpha$ radiation ($\lambda = 1.5418$ Å) in flat plate $\theta/2\theta$ geometry. Data were collected in the range of 5–110° 2θ in steps of 0.02° with a scan time of 10 s per step. Data were corrected for flat plate absorption prior to refinement. No preferred orientation was observed in the diffraction pattern.

Powder neutron diffraction data were collected on the HRPD diffractometer at ISIS, Rutherford Appleton Laboratory. Data were collected at 298 K in the time of flight range of 20–120 ms. The sample was placed in a 12-mm-diameter V can at the 1-m position, and 200 μA was collected in backscattering mode using ZnS detectors.

[1] To whom correspondence should be addressed. Fax: +44 (0) 181 981 8745: E-mail: i.abrahams@qmw.ac.uk.

0022-4596/99 $30.00

TABLE 1
Crystal and Refinement Parameters for $Bi_2Al_4O_9$

Chemical formula	$Bi_2Al_4O_9$
Formula weight	669.88
Crystal system	Orthorhombic
Space group	*Pbam* (No. 55)
Unit cell dimensions	$a = 7.7134(1)$, $b = 8.1139(2)$, $c = 5.6914(1)$ Å
Volume	356.20(2) Å^3
Z	2
Density (calculated)	6.248 g cm^{-3}
Absorption coefficient μ (Cu$K\alpha$ X-ray)	101.19 mm^{-1}
$F(000)$	580
Sample description	Yellow powder
R factors[a]	(a) X-ray $R_p = 0.1162$, $R_{wp} = 0.1709$, $R_{ex} = 0.0452$, $R_{F^2} = 0.1104$ (b) Neutron $R_p = 0.1100$, $R_{wp} = 0.1144$ $R_{ex} = 0.0324$, $R_{F^2} = 0.1442$
Total No. of variables	86
No of profile points used	4999 (X-ray) 6890 (neutron)

[a] For definition of R factors see Ref. (18).

Structure refinement was carried out using the Rietveld method with a combined X-ray and neutron approach. All calculations were performed using GSAS (5) with scattering factors for neutral atoms assumed in the X-ray refinement. A starting model for refinement was based on the single-crystal study of $Bi_2Al_4O_9$ (3). Cell dimensions and structural parameters were refined using both profiles, with independent refinement of profile parameters, i.e., peak shapes, background parameters, zero point corrections, and scale factors. A small amount of α-Al_2O_3 was refined as an impurity phase. In the final refinement anisotropic thermal parameters were refined for all atoms in the primary phase. Crystal and refinement parameters are summarized in Table 1. The final refined parameters are shown in Table 2, with selected bond lengths and angles in Table 3. The corresponding fitted diffraction profiles are shown in Fig. 1.

TABLE 2
Final Refined Parameters for $Bi_2Al_4O_9$

Atom	Wyc.	x	y	z	U_{eqv} (Å^2)[a]
Bi	4*g*	0.1711(1)	0.1677(1)	0.0(−)	0.0207(5)
Al(1)	4*f*	0.5(−)	0.0(−)	0.2645(6)	0.020(2)
Al(2)	4*h*	0.3545(4)	0.3399(4)	0.5(−)	0.022(2)
O(1)	2*b*	0.0(−)	0.0(−)	0.5(−)	0.030(2)
O(2)	8*i*	0.3718(2)	0.2056(2)	0.2503(3)	0.022(7)
O(3)	4*h*	0.1364(3)	0.4120(2)	0.5(−)	0.022(11)
O(4)	4*g*	0.1421(3)	0.4312(2)	0.0(−)	0.021(11)

[a] U_{eqv} is defined as one-third of the orthogonalized U_{ij} tensor.

TABLE 3
Significant Distances (Å) and Angles (°) in $Bi_2Al_4O_9$

Bi–O(2)	2.126(2) × 2
Bi–O(4)	2.149(2)
Bi–O(4)′	2.400(2)
Al(1)–O(2)	1.941(1) × 2
Al(1)–O(3)	1.848(3) × 2
Al(1)–O(4)	1.944(3) × 2
Al(2)–O(1)	1.717(3)
Al(2)–O(2)	1.796(2) × 2
Al(2)–O(3)	1.781(3)
O(2)–Bi–O(2)′	84.14(8)
O(2)–Bi–O(4)	86.09(6) × 2
O(2)–Bi–O(4)	71.24(5) × 2
O(4)–Bi–O(4)′	149.06(5)
O(2)–Al(1)–O(2)′	175.3(2)
O(2)–Al(1)–O(3)	94.1(1) × 2
O(2)–Al(1)–O(3)′	89.3(1) × 2
O(2)–Al(1)–O(4)	85.8(1) × 2
O(2)–Al(1)–O(4)′	90.5(1) × 2
O(3)–Al(1)–O(3)′	87.0(2)
O(3)–Al(1)–O(4)	97.4(1) × 2
O(3)–Al(1)–O(4)′	173.7(1) × 2
O(4)–Al(1)–O(4)′	78.5(2)
O(1)–Al(2)–O(2)	114.2(1) × 2
O(1)–Al(2)–O(3)	111.7(1) × 2
O(2)–Al(2)–O(2)	104.6(2)
O(2)–Al(2)–O(3)	105.6(1) × 2

A thermal ellipsoid plot of the $Bi_2Al_4O_9$ (ORTEP (6)) structure is shown in Fig. 2. Polyhedral structure plots were generated using STRUPLO for Windows (7).

Solid State ^{27}Al NMR

^{27}Al magic angle spinning (MAS) solid state NMR data were collected at 156.4 MHz on a Bruker AMX-600 spectrometer using a 4-mm outer diameter rotor and a spin rate of 13.11 kHz. The pulse width was 0.7 μs corresponding to a flip angle $\pi/12$, which is sufficiently small to allow quantification of the ^{27}Al spectrum (8). The ^{27}Al spectrum was simulated using the program QUASAR (9). For each transient, 25,000 points were acquired, with an acquisition time of 0.02 s, a relaxation delay of 0.25 s, and a sweep width of 62.5 kHz. Typically, 1000–2000 transients were accumulated for each spectrum and the first 16,384 data points were Fourier transformed. Chemical shifts are reported with the high frequency positive convention and are referenced to external 1 M aqueous Al^{3+}.

RESULTS AND DISCUSSION

A polyhedral representation of the $Bi_2Al_4O_9$ structure is shown in Fig. 3. The structure is built up of columns of

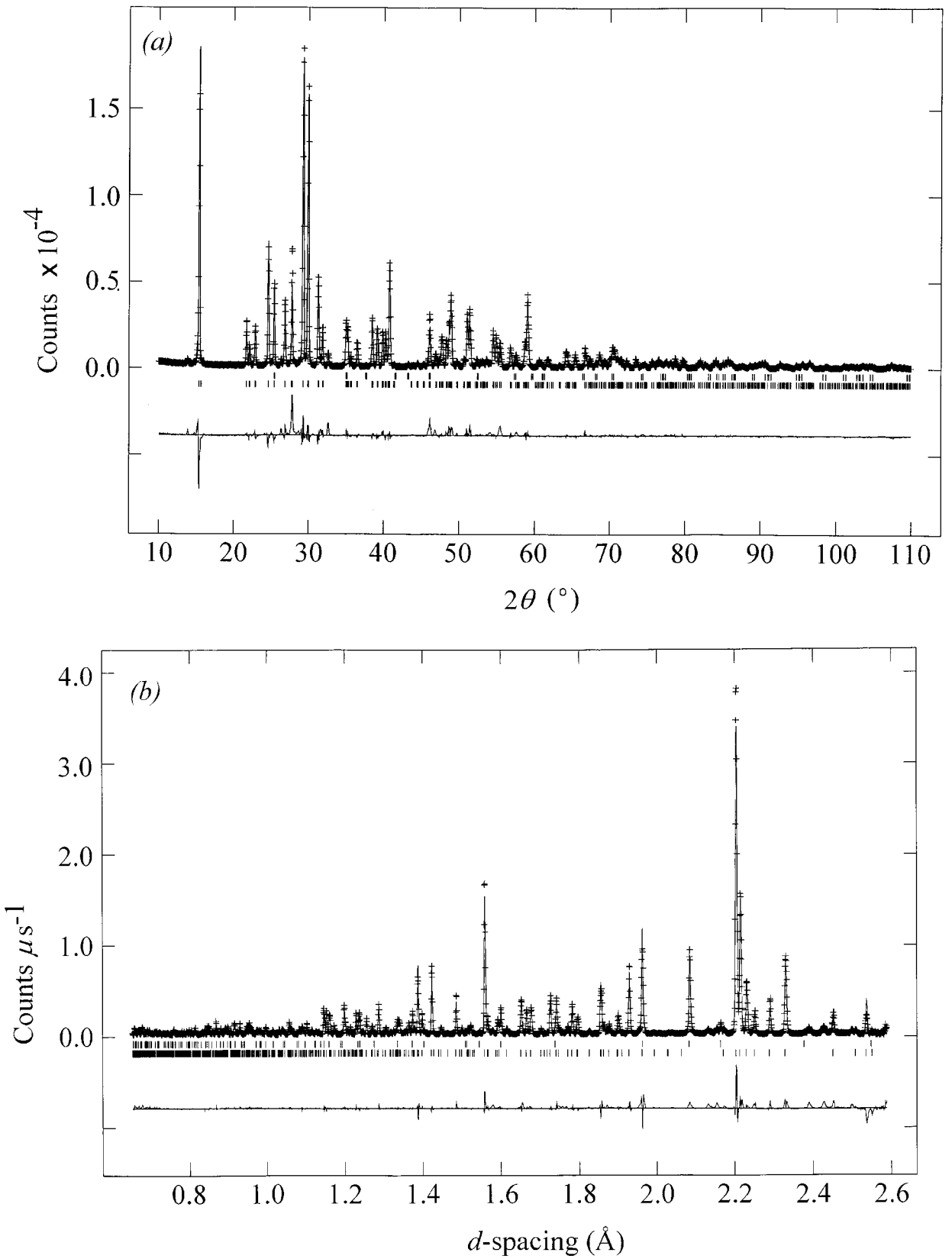

FIG. 1. Final fitted X-ray (a) and neutron (b) diffraction profiles for $Bi_2Al_4O_9$ showing observed (points), calculated (line), and difference (bottom) profiles. The reflection positions are indicated by markers (top, α-Al_2O_3; bottom, $Bi_2Al_4O_9$).

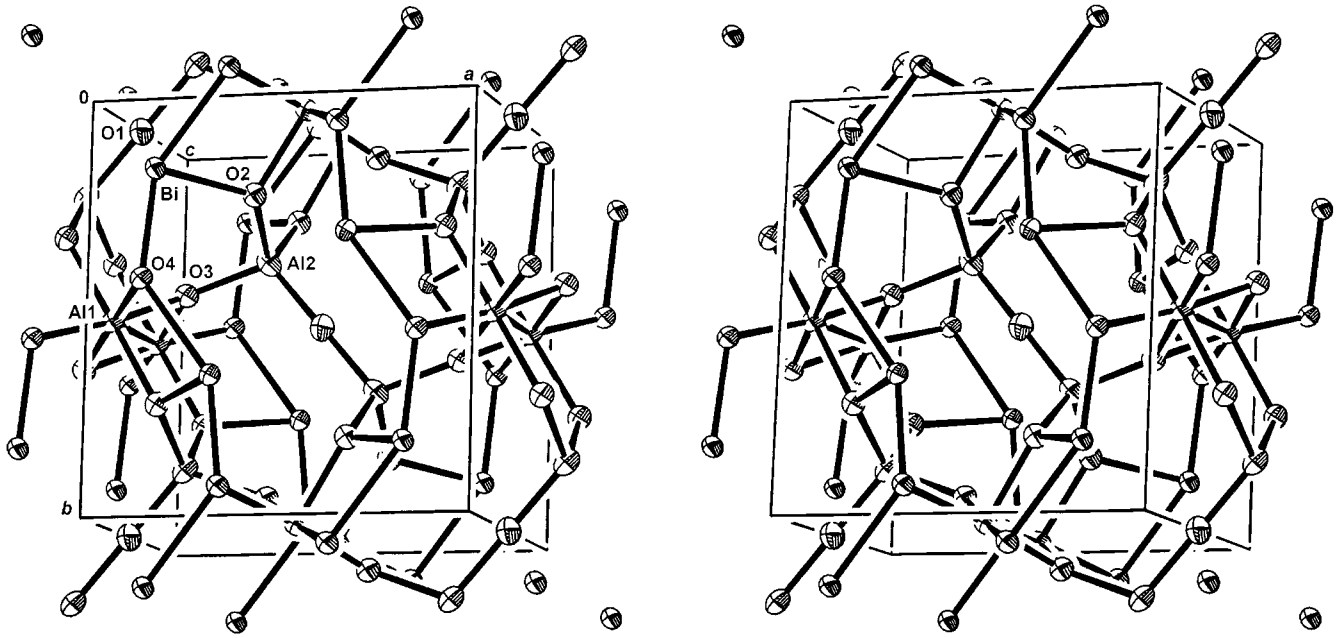

FIG. 2. Stereographic thermal ellipsoid plot for $Bi_2Al_4O_9$ (50% probability).

edge-sharing octahedra running parallel to the *c*-axis. The columns are linked by pairs of apex-sharing AlO_4 tetrahedra. Bi atoms are located in channels between the polyhedra, where they exhibit stereochemical activity of the nonbonding pair of valence electrons.

The aluminum atoms located in the Al(1) sites are in distorted octahedral co-ordination with oxygen. The Al(1)–O distances, 1.848–1.944 Å, compare with values of 1.856–1.974 Å in α-Al_2O_3 (10). The distances are slightly longer than those reported by Niizeki and Wachi (3) for $Bi_2Al_4O_9$. The tetrahedral Al(2) position has Al–O distances in the range 1.717–1.796 Å, which are typical for this coordination and can be compared with those in θ-Al_2O_3 (1.696–1.815 Å) (11), γ-Al_2O_3 (1.777 Å) (12), and η-Al_2O_3 (1.651–1.813 Å) (12). It is possible to calculate a distortion index D_{Ind} for the AlO_4 tetrahedra, where

$$D_{\text{ind}} = \frac{\sum_{i=1}^{i=6} (\theta_i - 109.17)^2}{6}.$$

Low values (<10) indicate small distortion, whereas high values (>20) indicate large distortions from regular tetrahedral geometry. A D_{Ind} value of 17.230 is calculated for the Al(2) tetrahedron in $Bi_2Al_4O_9$, indicating an intermediate level of tetrahedral distortion, which is probably caused by the asymmetric coordination of Bi in the structure.

The Bi atoms are in a distorted square pyramidal coordination environment, with three Bi–O bond lengths between 2.126 and 2.149 Å and a fourth longer contact at 2.400 Å. These values compare favorably with the distances 2.133–2.219 Å (fourth contact at 2.546 Å) and 2.130–2.283 Å (fourth contact at 2.422 Å) for the two Bi sites found in α-Bi_2O_3 (13). The range in the three short Bi–O values found in the present study is slightly smaller than that reported by Niizeki and Wachi at 2.11–2.18 Å in the same

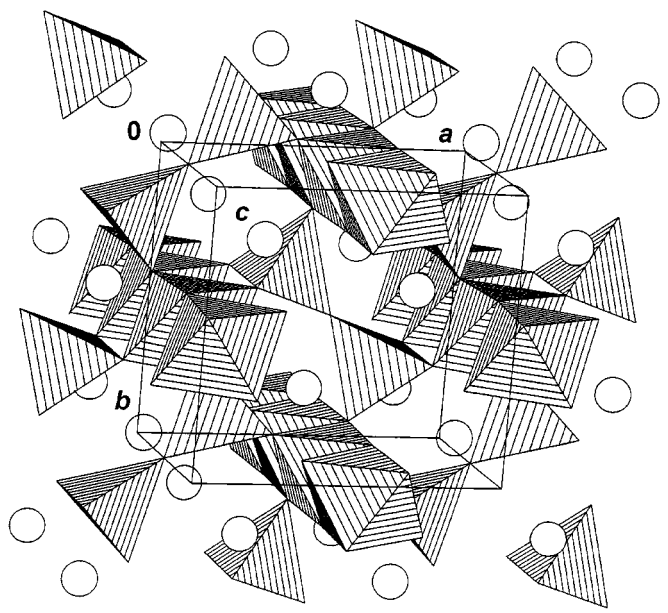

FIG. 3. Polyhedral projection of $Bi_2Al_4O_9$. AlO_6 and AlO_4 polyhedra are shown, Bi atoms are indicated by open circles.

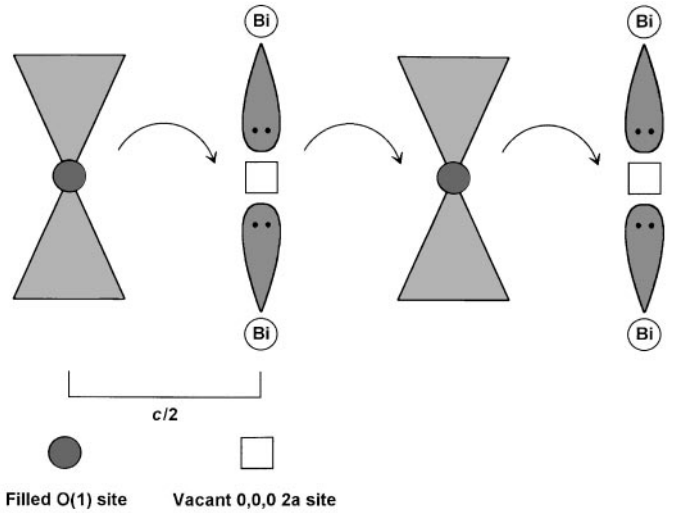

FIG. 4. Schematic representation of proposed one dimensional conductivity mechanism in $Bi_2Al_4O_9$. Triangles represent AlO_4 terahedra.

TABLE 4
Refined Anisotropic Thermal Parameters (Å^2) for $Bi_2Al_4O_9$

Atom	U_{11}	U_{22}	U_{33}	U_{12}	U_{13}	U_{23}
Bi	0.0163(5)	0.0183(5)	0.0274(5)	0.0016(5)	0.0(−)	0.0(−)
Al(1)	0.024(2)	0.019(2)	0.017(2)	0.004(1)	0.0(−)	0.0(−)
Al(2)	0.026(2)	0.026(2)	0.015(2)	0.007(2)	0.0(−)	0.0(−)
O(1)	0.022(2)	0.030(2)	0.037(2)	0.001(1)	0.0(−)	0.0(−)
O(2)	0.0228(7)	0.0238(7)	0.0181(7)	0.0012(6)	−0.006(6)	0.003(6)
O(3)	0.023(1)	0.022(1)	0.021(1)	0.0012(9)	0.0(−)	0.0(−)
O(4)	0.019(1)	0.019(1)	0.024(1)	− 0.0019(7)	0.0(−)	0.0(−)

compound (3). The asymmetric Bi coordination found in $Bi_2Al_4O_9$ suggests that the Bi $6s^2$ lone pair of valence electrons point toward the vacant 0, 0, 0 site.

If we consider the oxygen sublattice to be close packed, then anion vacancies occur above and below O(1) (in the *c*-axis direction) in the 2*a* site at 0, 0, 0, which gives a total of two vacancies per cell. The site is equidistant between two Bi atoms at 1.895 Å. However, it is likely that this site is high in energy with the Bi $6s^2$ lone pairs appearing to point directly toward it.

The conductivity mechanism (Fig. 4) is therefore likely to involve hopping of O(1) via the 2*a* sites. As there are no apparent intrinsic vacancies on the O(1) site, the mechanism is likely to involve the cooperative motion of oxide ions as seen in many other systems. The hopping distance is equivalent to *c*/2, i.e., 2.846 Å, with two hops required to reach an equivalent site. This proposed one-dimensional conductivity mechanism (along the *c*-axis vector) is supported by the fact that the U_{33} anisotropic thermal parameter of O(1), which describes the thermal vibration of this atom along the *c*-axis vector, is significantly higher than the U_{11} and U_{22} parameters (Table 4). All other oxygens in the structure have lower values for their thermal parameters. Clearly the mechanism relies on the polarizabilty of the Bi $6s^2$ lone pairs.

The ^{27}Al NMR pattern for $Bi_2Al_4O_9$ is shown in Fig. 5a. Two peaks are observed, cenetred at ca. 12 and 58 ppm. Iterative simulation of the spectrum (Fig. 5b) gave the parameters shown in Table 5, with the lower frequency peak best fitted as a superposition of two closely spaced resonances. The apparent peak positions are at lower frequencies than the true chemical shifts because of the second order quadrupolar effect (14). The major peak at 17.7 δ (apparent at 12 ppm) is assigned to six-coordinate Al (15). The peak at 66.9 δ (apparent at 58 ppm) is well within the range reported for tetrahedrally coordinated Al (16). Equal populations for the octahedral and tetrahedral Al sites are predicted from the crystal structure data and this is reflected in the approximately equal intensities of the resonances at 17.7 and 66.9 δ. The third, minor resonance at 16.1 δ is most likely due to α-Al_2O_3, since this contaminant was seen in the diffraction patterns and a single ^{27}Al resonance is reported for α-Al_2O_3, at 12.3 ppm (uncorrected for the second order quadrupole effect) (17). The percentage intensity of this resonance (Table 5) indicates that an upper limit of 6 mol% of the total Al present in the sample is in the form of α-Al_2O_3. The value for the quadrupole coupling constant, C_q, for the tetrahedral Al(2) site is 5.2 MHz, which is within the range (2–13 MHz) determined by Müller *et al.* (15) for tetrahedral Al in

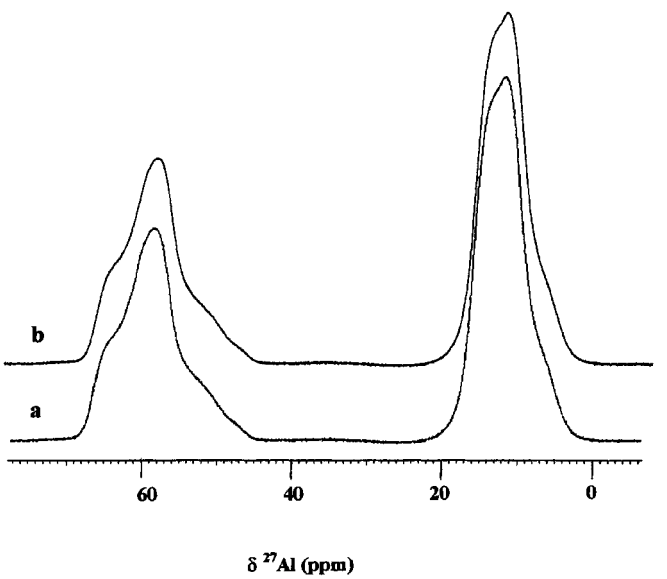

FIG. 5. Experimental (a) and simulated (b) 156.38 MHz ^{27}Al MAS NMR spectra of $Bi_2Al_4O_9$.

TABLE 5
^{27}Al NMR Parameters for $Bi_2Al_4O_9$ Derived by Iterative Simulation[a]

Site	% Intensity	δ_{iso}	C_q (MHz)	η_q
Al(1) oct	47	17.7(2)	4.8(1)	0.61(15)
Al(2) tet	41	66.9(3)	5.2(1)	0.77(9)
Al(3) (Al_2O_3)	12	16.1(3)	3.5(1)	0.21(4)

Note. Estimated standard deviations are given in parentheses.

[a] δ_{iso} is the isotropic chemical shift, C_q is the quadrupole coupling constant, and η_q is the asymmetry parameter. Chemical shifts are referred to an external 1 M Al^{3+} solution.

polycrystalline CaO/Al_2O_3 materials. However, the value of C_q, estimated here for the octahedral Al(1) site at 4.8 ± 0.1 MHz, is considerably larger than the values (<1–2.0 MHz) found by Müller *et al.* (15) for the corresponding Al sites in the CaO/Al_2O_3 system.

ACKNOWLEDGMENTS

We gratefully acknowledge the EPSRC for a project studentship to A.J.B. We also thank the University of London Intercollegiate Research Services for access to NMR facilities and Dr. A. Aliev for his help in NMR data collection. We are also indebted to Dr. I. Gibson at the IRC in Biomedical Materials for collecting the X-ray data.

REFERENCES

1. J. B. Goodenough, A. Manthiram, P. Paranthaman, and Y. S. Zhen, *Solid State Ionics* **52,** 105 (1992).
2. E. I. Speranskaya, V. M. Skorikov, G. M. Safronov, and E. N. Gaidukov, *Izv. Akad. Nauk SSSR, Neorganiicheskie Materialy* **6,** 1364 (1970).
3. N. Niizeki and M. Wachi, *Z. Krystallogr.* **127,** 173 (1968).
4. I. Bloom, M. C. Hash, J. P. Zebrowski, K. M. Myles, and M. Krumpelt, *Solid State Ionics* **53–56,** 739 (1992).
5. A. C. Larson, and R. B. Von Dreele, "Los Alamos National Laboratory Report, No. LAUR-86-748," 1987.
6. L. J. Farrugia, *J. Appl. Crystallogr.* **30,** 565 (1997).
7. L. J. Farrugia, STRUPLO for Windows, University of Glasgow, 1998.
8. D. Fenzke, D. Freude, T. Fröhlich, and J. Haase, *Chem. Phys. Lett.* **111,** 171 (1984).
9. J. P. Amoureux, C. Fernandez, L. Carpentier, and E. Cochon, *Phys. Status Solidi* **A132,** 461 (1992).
10. D. E. Cox, A. R. Moodenbough, A. W. Sleight, and H. Y. Chen, *U.S. National Bureau of Standards, Special Publication* **562,** 567 (1980).
11. E. Husson and Y. Repelin, *Eur. J. Solid State Inorg. Chem.* **33,** 1223 (1996).
12. R-S. Zhou and R. L. Snyder, *Acta Crystallogr. Sect. B* **47,** 617 (1991).
13. H. A. Harwig, *Z. Anorg. Allg. Chem.* **444,** 151 (1978).
14. E. Lippmaa, A. Samoson, and M. Mägi, *J. Am. Chem. Soc.* **108,** 1730 (1986).
15. D. Müller, W. Gessner, A. Samson, E. Lippmaa, and G. Scheler, *Polyhedron* **5,** 779 (1986).
16. D. Müller, W. Gessner, A. Samson, E. Lippmaa, and G. Scheler, *J. Chem. Soc. Dalton Trans.* 1277 (1986).
17. A. E. Hughes, S. Rajendran, and M. E. Smith, *Mater. Lett.* **17,** 303 (1993).
18. R. A. Young (Ed.), "The Rietveld Method," IUCR Monographs on Crystallography, Vol. 5, p. 21. Oxford Univ. Press, New York, 1993.